

# The Maximally Embedded $H(V)$ -parallelogram is at Least $2/9$ of the Convex Region

Xuelei (Sherry) Ni and Xiaoming Huo <sup>a</sup>

October 10, 2005

## Abstract

The proportion of a maximally embedded  $h(v)$ -parallelogram in a convex region is proved to be at least  $2/9$  in area. This study is motivated by a multiscale method of detecting the presence of a convex inhomogeneous region in a Gaussian random field. Such a constant ( $2/9$ ) reveals the feasibility and effectiveness of using a multiscale algorithm in detecting the presence of a convex-shaped inhomogeneous region. This is a supporting document of a formal paper [5], and is a part of a thesis [6].

**Key Words and Phrases.** Convex regions, detectability, image detection.

**Acknowledgements.** This work has been partially supported by National Science Foundation grants DMS 0140587 and DMS 0346307.

<sup>a</sup>: School of Industrial and Systems Engineering, Georgia Institute of Technology, Atlanta, GA 30332-0205. {xni, xiaoming}@isye.gatech.edu

## 1 Introduction

An  $h(v)$ -parallelogram is introduced in [1], which addresses the problem of detecting the presence of a range of geometric objects efficiently in an image that is contaminated with white Gaussian noise. In this technical report, we analyze the relationship between the  $h(v)$ -parallelograms and convex regions. The application of our result is to describe the detectability of convex inhomogeneous regions in a noisy image [5].

It has been shown in [6] that the number of convex sets (equivalently, regions) in a digital image grows faster than any finite-degree polynomial of  $n$ , where the image size is  $n \times n$ . Hence enumerating the convex regions will not render an efficient algorithm to detect the inhomogeneous convex regions in a image.  $H(V)$ -parallelograms are easy to be investigated: The number of  $h(v)$ -parallelograms is a polynomial of  $n$  and they can be enumerated by some fast algorithms. If we can find the connection between  $h(v)$ -parallelograms and convex regions, we can detect a convex inhomogeneous region *indirectly* by using  $h(v)$ -parallelograms as surrogates. In [5], such a connection is established. In particular, the existence of a positive

constant  $2/9$  reveals the asymptotic equivalence of the two problems – we refer to [5] for details. The proof of the constant  $2/9$  is long and tedious, not suitable to be presented in a regular paper. We decide to use this technical report to document it.

We start with the definition of an  $h(v)$ -parallelogram.

**Definition 1 ( $h(v)$ -parallelogram).** *An  $h$ - (resp.  $v$ -)parallelogram is a parallelogram having two sides horizontal (resp. vertical) and its horizontal (resp. vertical) projection to the  $y$ - (resp.  $x$ -) axis on a Cartesian plane is a dyadic interval.*

A dyadic interval is defined as follows. We assume that the size of the image  $n = 2^m$ , for some integer  $m$ . Note there is a one-to-one mapping between the index set of pixels from  $\{0, 1, \dots, n-1\}$  to  $\{0, 1/2^m, 2/2^m, \dots, 1-1/2^m\}$ . A dyadic interval as a subinterval of interval  $(0, 1)$  is defined as follows.

**Definition 2 (dyadic interval).** *Interval  $(a, b)$  is a dyadic interval if and only if there exist two non-negative integers  $s$  and  $\ell$ ,  $s \leq m$  and  $\ell < 2^s$ , such that  $a = \ell/2^s$  and  $b = (\ell + 1)/2^s$ .*

In the discrete case, recalling the above one-to-one mapping, a subsequence starting at  $i$  and ending at  $j$ ,  $i \leq j$  corresponds to the interval  $(i/n, (j + 1)/n)$ .

The total number of  $h(v)$ -parallelograms is  $O(n^4)$ . In comparison, recall that the cardinality of all convex regions is higher than any finite degree polynomial of  $n$ . We count the number of  $h(v)$ -parallelograms. At resolution  $n$ , i.e., in an  $n$  by  $n$  image, there are  $O(n)$  dyadic intervals, including both vertical and horizontal ones. For each dyadic interval, there are at most  $O(n^3)$   $h$ (or  $v$ )-parallelograms: there are  $O(n)$  choices at both lower corners in both sides of the dyadic interval; the height of the parallelogram adds another  $O(n)$  complexity.

In fact, a lower order enumerating algorithm can be derived by using a multiscale methodology with the help of Beamlets and Beamlet algorithms [1]. An algorithm with order of complexity  $O(n^2 \log^2(n))$  in detecting an  $h(v)$ -parallelogram is reported in [1]. Fast algorithms are not the focus of this technical report. We will not pursue in this direction.

In the rest of this report, we present the main result of the minimax proportion in Section 2, the proof of the main result in Section 3, and some discussion in Section 4.

## 2 The Minimum Proportion of the Maximally Embedded $H(V)$ -parallelogram

The relationship between a convex set and its embedded  $h(v)$ -parallelogram is stated as follows.

**Theorem 3 (Main Result).** *For any convex set, there is an embedded  $h$ - or  $v$ - parallelogram, which occupies at least  $2/9$  of the convex set. Moreover, the constant  $2/9$  can not be increased. In other words, for any quantity that is greater than  $2/9$ , there is a convex set, within which there is no embedded  $h$ - or  $v$ - parallelogram that takes  $2/9$  in area of the convex set.*

This theorem is proved in continuum. In the discrete case, when the resolution  $n \rightarrow \infty$ , the same quantity holds.

### 3 Proof

The main theorem is proved in this section. We should consider both h-parallelograms and v-parallelograms. However, due to the symmetry of convex sets, only one type of parallelograms need to be considered. If we consider v-parallelogram alone, the minimax proportion  $2/9$  can be reached. One such limit case is shown in Figure 1. Without loss of generality, v-parallelograms are considered in the sequel.

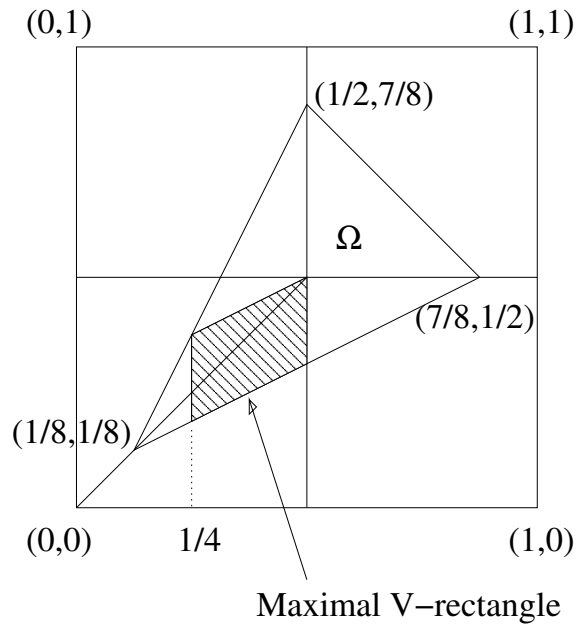


Figure 1: An example when minimax embedding  $2/9$  is achieved.

#### 3.1 Different Cases

A maximally embedded v-parallelogram is illustrated in Figure 2. Note that we do not use the word ‘inscribed’, to reflect the possibility that one corner point of a parallelogram may not be on the boundary of a convex set.

To simplify the proof, we assume that one side of the convex set is horizontal. An *affine transform* can be applied to convert an arbitrary convex set into a convex set with a horizontal side, as illustrated in Figure 3: the original set is  $\Omega$ , and the transformed set is  $\Omega'$ . Note the two sets have the same height at the same location. It is not hard to verify that  $\Omega'$  is convex. Moreover, a maximally embedded v-parallelogram in  $\Omega$  becomes a Maximally

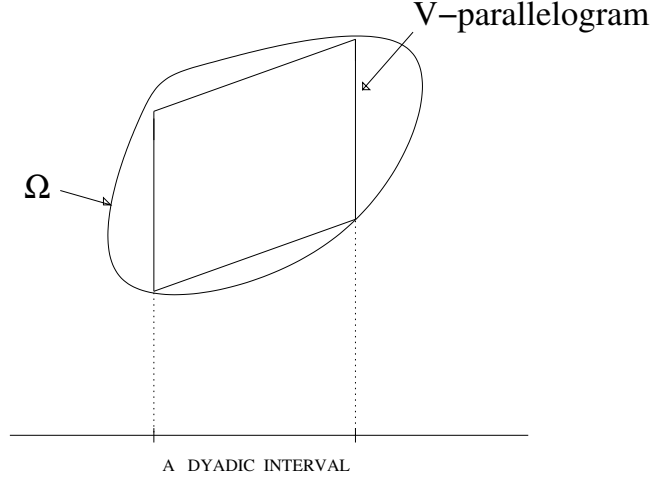


Figure 2: Illustration of a maximally embedded v-parallelogram

Embedded Rectangle (MER) in  $\Omega'$ . Note that the rectangle must be supported by a dyadic interval on the x-axis, due to the definition of the v-parallelogram.

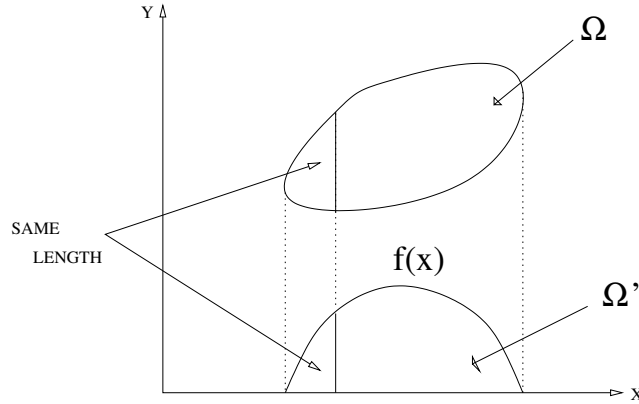


Figure 3: Illustration of the transformation, which transforms an arbitrary convex set into a convex set with a horizontal side.

The essence of the proof is to enumerate all the configurations of a convex set. We consider the horizontal side of a (transformed) convex set. Let  $a$  denote a dyadic number: i.e., there exist two integers  $s$  and  $\ell$ ,  $\ell < 2^s$ , such that  $a = \ell/2^s$ . Let  $\delta = 1/2^{s'}$ ,  $s' \geq s - 1$ . Note that intervals  $(a, a + 0.5\delta)$  and  $(a + 0.5\delta, a + \delta)$  are two dyadic intervals. For  $(a, a + \delta)$ , it is a dyadic interval when  $s' \geq s$ , and may not be when  $s' = s - 1$ . We can always find an  $a$  and a  $\delta$  such that (the horizontal side of)  $\Omega'$  is complete inside of interval  $(a, a + \delta)$ , as shown in Figure 4 (a). We denote this case as TC-1. Now, if we consider the middle point  $a + 0.5\delta$ , there are two possibilities:

1. If the middle point  $a + 0.5\delta$  is outside  $\Omega'$ , say, it is on the left of  $\Omega'$ , then by setting

$a^{\text{new}} = a + 0.5\delta$  and  $\delta^{\text{new}} = \delta/2$ , we go back to case TC-1 in Figure 4 (a). The case when  $a + 0.5\delta$  is on the right of  $\Omega'$  can be similarly transferred to TC-1.

2. Therefore, we only need to consider the case when the middle point is inside  $\Omega'$  (Figure 4 (c) TC-3).

Now we consider two more quarter points:  $a + \delta/4$  and  $a + 3\delta/4$ . If none of them is inside  $\Omega'$ , which is illustrated in Figure 4 (d), let  $a^{\text{new}} = a + \delta/4$  and  $\delta^{\text{new}} = \delta/2$ , we can transfer it back into case TC-3 in Figure 4 (c). So we only need to consider the case in which at least one of the above two points is inside  $\Omega'$ . These two cases are illustrated in Figure 4 (e), in which both are inside, and Figure 4 (f), in which only one is inside. They are called cases C1 and C2, respectively, and will be investigated further.

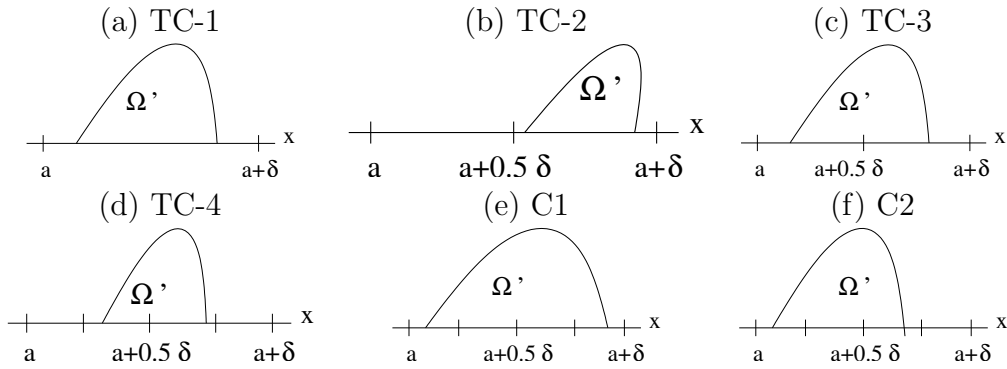


Figure 4: Possible cases while projecting to the x-axis. TC stands for Temporary Case.

We consider the MER. To reduce ambiguity, if there are two (embedded) rectangles with equal area, we always choose the one with larger support. Based on the definition of v-parallelgram, the support of MER (on the boundary of  $\Omega'$  on x-axis) is a dyadic interval.

Within the case of C1, there are six subcases, as in the following table. The notations of points are illustrated in Figure 5. Note that there is a rescaling on the x-axis:  $\delta^{\text{new}} = \delta/4$ .

- C1-1: the support of the MER is with length  $\leq \delta/4$ , e.g., rectangle  $P_{11}P_{12}P_{46}P_{45}$ .
- C1-2: the support of the MER is with length  $\delta$ , i.e., the support is  $(a + \delta, a + 2\delta)$  or  $(a + 2\delta, a + 3\delta)$ . Due to symmetry, we only need to consider the MER with support  $(a + \delta, a + 2\delta)$ , which is rectangle  $P_{31}P_{32}P_{44}P_{42}$  in the figure.
- C1-3: the support of the MER is with length  $\delta/2$ . This item and the next two cover this case. Due to symmetry, other locations are automatically taken care of. In this subcase, the MER is rectangle  $P_{21}P_{22}P_{42}P_{41}$ .
- C1-4: the support of the MER is with length  $\delta/2$  and the MER is  $P_{22}P_{23}P_{43}P_{42}$ .
- C1-5: the support of the MER is with length  $\delta/2$  and the MER is  $P_{23}P_{24}P_{44}P_{43}$ .

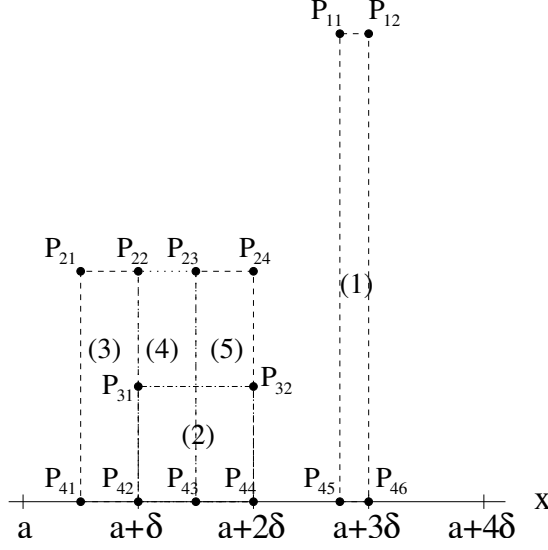


Figure 5: Subcases of Case C1.

Within C2, there are nine subcases, as illustrated in Figure 6.

C2-1: the support of the MER is with length  $\leq \delta/8$ , e.g. rectangle  $P_{11}P_{12}P_{59}P_{58}$ .

C2-2: the support of the MER is with length  $\delta$ . The only possibility is  $P_{41}P_{42}P_{57}P_{54}$ .

C2-3: the support of the MER is with length  $\delta/2$ . Due to symmetry, only two conditions need to be considered. In this subcase, we consider rectangle  $P_{31}P_{32}P_{54}P_{52}$ .

C2-4: continuing from the above subcase, the MER is the rectangle  $P_{32}P_{33}P_{56}P_{54}$ .

C2-5: the support of the MER is with length  $\delta/4$ . Due to symmetry, five possibilities need to be considered. In this subcase, the MER is  $P_{21}P_{22}P_{52}P_{51}$ .

C2-6: the MER is  $P_{22}P_{23}P_{53}P_{52}$ .

C2-7: the MER is  $P_{23}P_{24}P_{54}P_{53}$ .

C2-8: the MER is  $P_{24}P_{25}P_{55}P_{54}$ .

C2-9: the MER is  $P_{25}P_{26}P_{56}P_{55}$ .

### 3.2 Discussion Regarding the Foregoing Cases

We prove the theorem through all the above subcases. All the proofs are illustrated in figures.

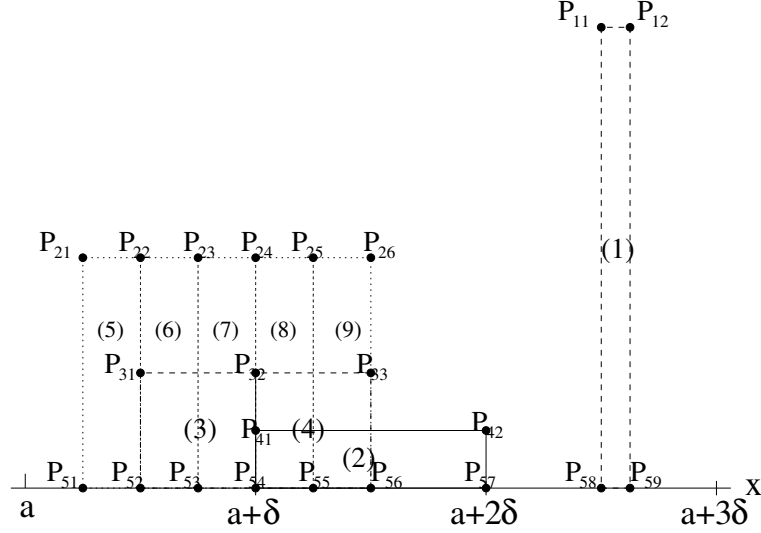


Figure 6: Subcases of case C2.

### 3.2.1 Case C1-1 and C2-1

For cases C1-1 and C2-1, it can be easily seen that these two subcases cannot exist. Actually, we can always find a contradiction. That is, inside the convex set, we can find other rectangles with dyadic supports and larger areas. These are illustrated in Figure 7 and 8, respectively.

To be more specific, we consider case C1-1 first. Under C1-1, the area of the MER candidate, rectangle  $P_{11}P_{12}P_{46}P_{45}$ , is less than or equal to  $h\delta/4$  (shaded parts in Figure 7), where  $\delta/4$  is the upper bound of the width and  $h$  is the height. The support can be either in interval  $(a, a + \delta)$  or in  $(a + \delta, a + 2\delta)$ , which also includes the other two possibilities  $(a + 2\delta, a + 3\delta)$  and  $(a + 3\delta, a + 4\delta)$  because of symmetry.

- When the support is within interval  $(a + \delta, a + 2\delta)$ , this situation is illustrated in Figure 7 (a). From the definition of convex sets, it can be easily verified that the trapezoid with vertices  $(a + \delta, 0)$ ,  $P_{11}$ ,  $P_{12}$ , and  $(a + 3\delta, 0)$  is within the convex set  $\Omega'$ . Hence, the rectangle embedded in the trapezoid with support  $(a + \frac{3}{2}\delta, a + 2\delta)$  and one vertex on the line between  $(a + \delta, 0)$  and  $P_{11}$  is inside  $\Omega'$  as well. Note  $(a + \frac{3}{2}\delta, a + 2\delta)$  is a dyadic interval and the height of this new rectangle is greater than  $h/2$ , which leads to an area greater than  $h\delta/4$ . Hence,  $P_{11}P_{12}P_{46}P_{45}$  cannot be the MER.
- When the support is within interval  $(a, a + \delta)$ , as illustrated in Figure 7 (b), an rectangle with dyadic support  $(a + \delta, a + 2\delta)$  can be found embedded inside  $\Omega'$ . The height of this rectangle should be greater than  $h/3$  by elementary knowledge in geometry. Hence, this embedded rectangle has area greater than  $(h\delta/3)$ , which also leads to a contradiction.

From all the above, case C1-1 does not exist.

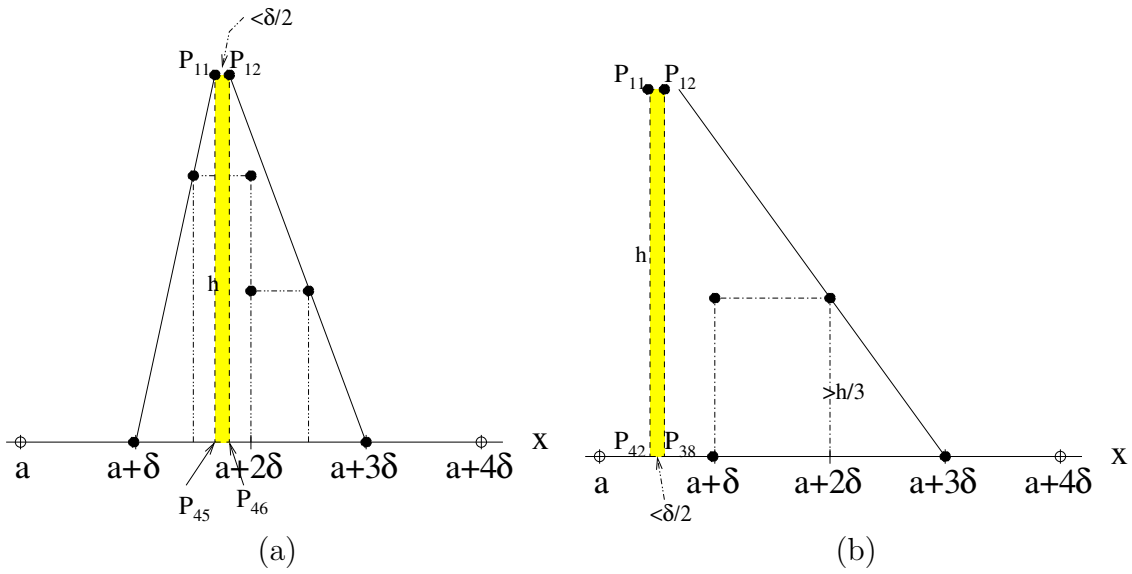


Figure 7: Case 1-1 cannot occur.

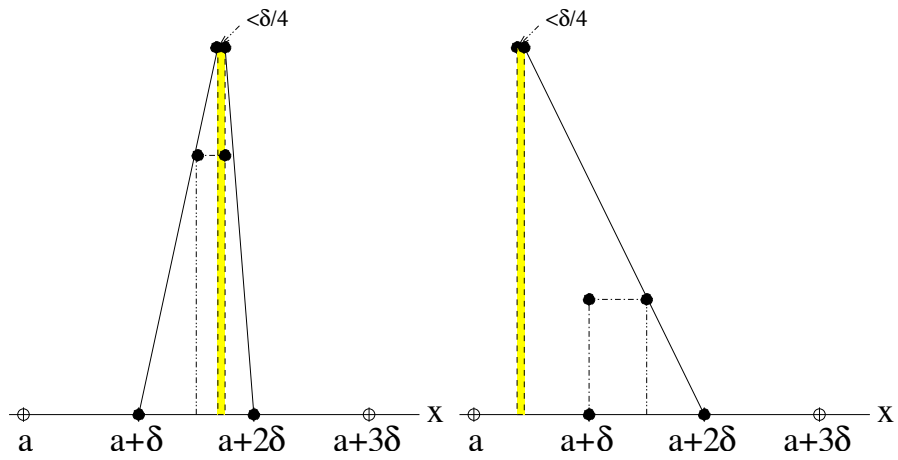


Figure 8: Case 2-1 cannot occur.

Similarly, under the conditions of C2-1, no embedded rectangle with a dyadic base shorter than  $\delta/8$  can be the MER, no matter where the rectangle is (cf. Figure 8).

### 3.2.2 Case C1-3 and C1-4

Cases C1-3 and C1-4 are similar with the above two cases C1-1 and C2-1. Under C1-3 (Figure 9 (a)), though, a shorter rectangle having the same area as the proposed MER can be found. The shorter rectangle also has a dyadic support and the original MER is shaded in the figure. Due to our preference for longer support, this one are embedded in another case. Under C1-4 (Figure 9 (b)), a larger embedded dyadic rectangle can be found.

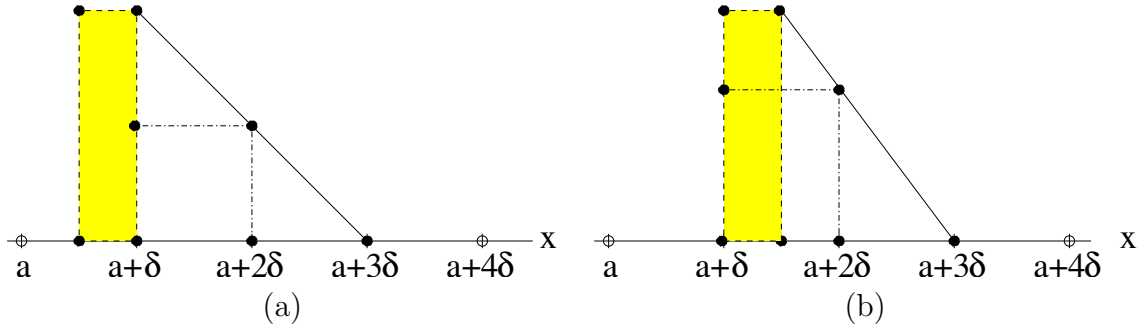


Figure 9: Case C1-3 & Case C1-4, where Case C1-3 can be covered by another case and Case C1-4 is impossible. The shaded areas are the original MERs. (a) is for C1-3 and (b) is for C1-4.

### 3.2.3 Case C1-2

Case C1-2 is much more complicated. We can divide this case further to get more detailed subcases. Figure 10 presents some key points that are important in the following discussion. In this figure and all the figures in the remaining of this report, a solid point means this point is inside or on the boundary of convex set  $\Omega'$ . A circle either denotes a point outside of  $\Omega'$ , or a point we're not sure whether it is inside or outside. Notations  $P_{ij}$  are used to denote these points. Points  $P_{i\times}$  are in the same height, while the height of points  $P_{4\times}$  (given it is not on the x-axis) is half of the height of points  $P_{3\times}$ . Similarly, the height of points  $P_{3\times}$  is half of the height of points  $P_{2\times}$ . For the horizontal inter-distance among  $P_{\times j}$ 's, if  $x_{i,j}$  denotes the x-coordinate of  $P_{ij}$ , then intervals  $(x_{i,j}, x_{i,j+1}), (x_{i,j+1}, x_{i,j+2})$  and so on are successive dyadic intervals with the same length. For the points at different level, the length of  $(x_{i,j}, x_{i,j+1})$  is half of the length of interval  $(x_{i+1,j}, x_{i+1,j+1})$ . Moreover,  $l_{ij}$  denotes a line passing through point  $P_{ij}$  such that  $\Omega'$  is on one side of the line.

Now we return to case C1-2. Given Figure 10, where the MER have two vertices  $P_{31}$  and  $P_{32}$ , we know that at least one of the points  $P_{31}$  and  $P_{32}$  will be on the boundary of  $\Omega'$ .

First, we assume  $P_{31}$  is on the boundary. Hence, line  $l_{31}$ , passing through  $P_{31}$ , can be chosen such that  $\Omega'$  is on the right side of  $l_{31}$ . Moreover,  $P_{33}$  should be on the boundary of  $\Omega'$

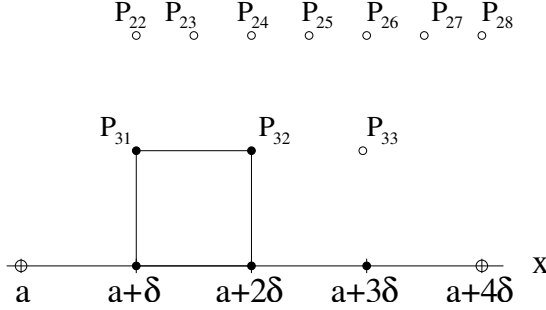


Figure 10: Case 1-2: an overview.

or  $P_{33} \notin \Omega'$ , i.e., it cannot be inside  $\Omega$ . Otherwise, we can find a larger embedded rectangle with dyadic support  $(a + 2\delta, a + 3\delta)$ . Furthermore, among  $P_{22}, P_{23}, P_{24}, P_{25}, P_{26}$  and  $P_{27}$ , at most one of them will be in the  $\Omega'$ . Otherwise, we will have a contradiction regarding the MER again. Hence, we will have several subcases depending on the status of each  $P_{2j}$ .

If  $P_{22} \in \Omega'$  (Figure 11), then  $l_{31} \perp X$  and  $P_{23} \notin \Omega'$ . Hence, we can find a line  $l_{23}$  such that  $\Omega'$  is on the left side of  $l_{23}$ . To make the possible  $\Omega'$  have the maximal area,  $l_{23}$  should pass  $P_{33}$  as well. The reason is the following. Clearly, the  $\Omega'$  with the maximal area is the triangle surrounded by  $l_{31}$ ,  $l_{23}$ , and x-axis, or the quadrangle surrounded by those three lines and the additional side vertical to x-axis and parsing through  $(a + 4\delta - \varepsilon, 0)$ . An offset  $\varepsilon$  is introduced because  $(a + 4\delta, 0) \notin \Omega'$ . In Figure 11 (a), point  $P_{33}$  is either on  $l_{23}$  or above it. Obviously, the polygon with one side passing through  $P_{33}$  has larger area. In Figure 11 (b) and (c),  $P_{33}$  is either on  $l_{23}$  or below it. Difference between (b) and (c) is that in (b), line  $l_{33}$  intersects with x-axis outside interval  $(a, a + 4\delta)$ ; in (c), line  $l_{33}$  intersects with x-axis inside interval  $(a, a + 4\delta)$ . Clearly, from the figures, both of (b) and (c) will give a larger  $\Omega'$  when  $P_{33}$  is on  $l_{23}$ . Hence, in this case, the maximal  $\Omega'$  is the quadrangle mentioned in this paragraph. We have, under this circumstance,

$$\frac{|MER|}{|\Omega'|} \geq \frac{1}{4} > \frac{2}{9}.$$

If  $P_{23} \in \Omega'$  (Figure 12), then  $P_{24} \notin \Omega'$ . Recall  $P_{31}$  is on the boundary of  $\Omega'$ . We have that  $\Omega'$  is on the right side of  $l_{31}$  and the left side of  $l_{24}$ . Through Figure 12 (a), we find that when the slope of  $l_{31}$  is increasing, the area of the possible  $\Omega'$  is increasing. Through Figure 12 (b), we find that  $l_{24}$  should pass through  $P_{33}$ . Hence,  $\Omega'$  is within the triangle bounded by the  $l_{31}$  that is vertical to the x-axis, the  $l_{24}$  that passes through  $P_{33}$  and the x-axis. Hence, in this case,

$$\frac{|MER|}{|\Omega'|} \geq \frac{2}{9}.$$

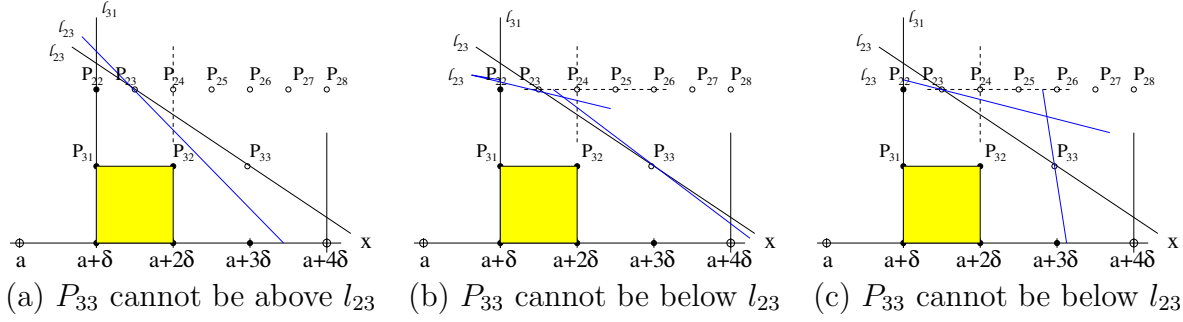


Figure 11: Subcase of Case 1-2, where  $P_{31}$  is on the boundary of  $\Omega'$  and  $P_{22} \in \Omega'$ . (a) demonstrates that  $P_{33}$  cannot be above  $l_{23}$ ; (b) demonstrates that  $P_{33}$  cannot be below  $l_{23}$  when  $l_{33}$  intersects with x-axis outside of interval  $(a, a + 4\delta)$ ; (c) demonstrates that  $P_{33}$  cannot be below  $l_{23}$  when  $l_{33}$  intersects with x-axis inside of interval  $(a, a + 4\delta)$ .

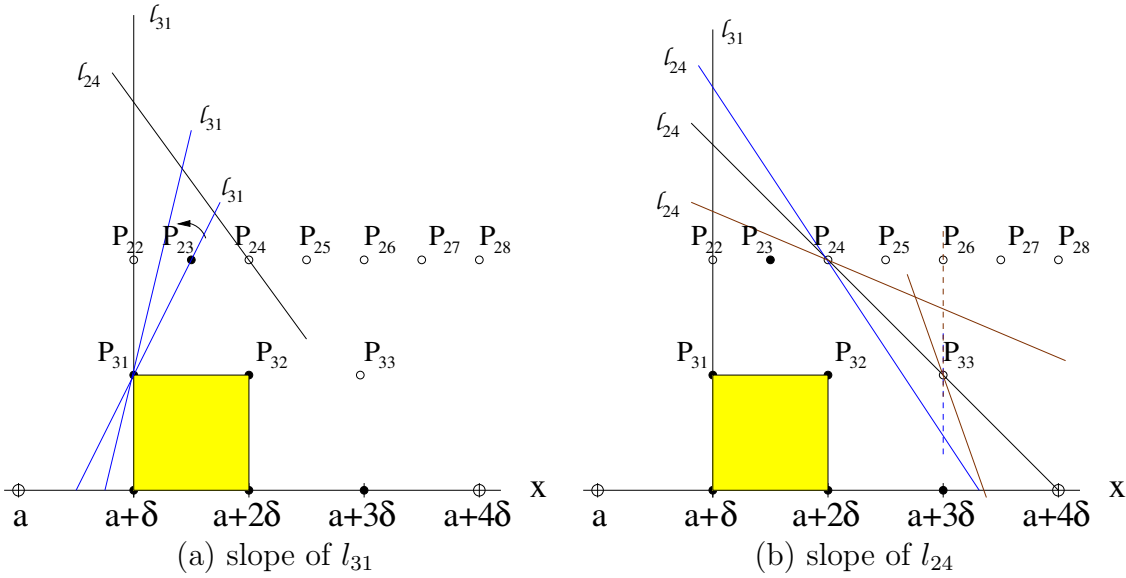


Figure 12: Subcase of Case 1-2, where  $P_{31}$  is on the boundary of  $\Omega'$  and  $P_{23} \in \Omega'$ . (a) demonstrates that the larger the slope of  $l_{31}$  is, the larger the possible  $\Omega'$  is; (b) demonstrates that  $P_{33}$  cannot be below or above  $l_{24}$  in order to make a larger feasible  $\Omega'$ .

If  $P_{24} \in \Omega'$  (Figure 13), we have  $P_{25} \notin \Omega'$ . Hence,  $\Omega'$  is on the right side of  $l_{31}$  and the left side of  $l_{25}$ . The maximal and applicable  $\Omega'$  should be within the triangle bounded by  $l_{31}$ ,  $l_{25}$ , and the x-axis, where  $l_{31}$  should pass through  $P_{23}$  (Figure 13 (a)) and  $l_{25}$  should pass through  $P_{33}$  (Figure 13 (b)). Therefore,

$$\frac{|MER|}{|\Omega'|} \geq \frac{2}{9}.$$

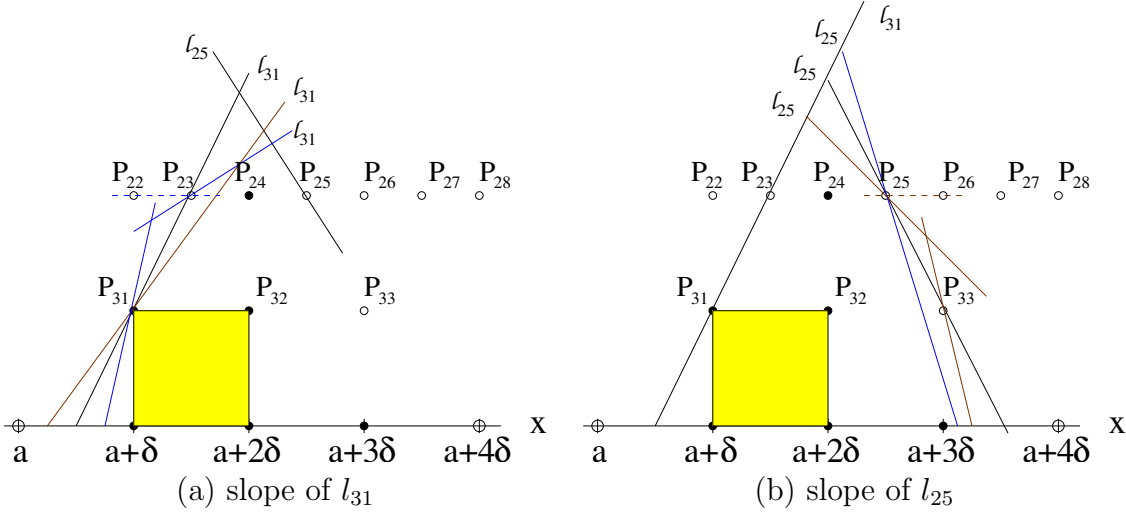


Figure 13: Subcase of Case 1-2, where  $P_{31}$  is on the boundary of  $\Omega'$  and  $P_{24} \in \Omega'$ . (a) demonstrates that  $P_{23}$  should not be below or above  $l_{31}$  in order to have a larger  $\Omega'$ ; (b) demonstrates that  $P_{33}$  should not be below or above  $l_{25}$  in order to have a larger  $\Omega'$ .

If  $P_{25} \in \Omega'$  (Figure 14),  $\Omega'$  is on the right side of  $l_{31}$  and the left side of  $l_{33}$ . We study  $l_{33}$  instead of  $l_{26}$  because  $P_{26} \notin \Omega'$ ,  $P_{33}$  is on the boundary of  $\Omega'$  or  $P_{33} \notin \Omega'$ , and  $P_{33}$  is exactly below  $P_{26}$ . We observe that the possible  $\Omega'$  is limited by  $l_{31}$ , which passes through  $P_{24}$  (Figure 14 (a)),  $l_{33}$ , which also passes through  $P_{26}$  (Figure 14 (b)), and the x-axis. Consequently, we have

$$\frac{|MER|}{|\Omega'|} \geq \frac{2}{9}.$$

If  $P_{26} \in \Omega'$  (Figure 15), we can prove that such a case is impossible by finding a larger dyadic rectangle in  $\Omega'$  with support  $(a + 2\delta, a + 3\delta)$ . The same thing will happen if  $P_{27} \in \Omega'$ .

If none of  $P_{2x} \in \Omega'$  (Figure 16). It is obvious that the maximal  $\Omega'$  is smaller than the previous subcases. Possible  $\Omega'$ 's are illustrated in the figure. Hence,

$$\frac{|MER|}{|\Omega'|} \geq \frac{1}{4} > \frac{2}{9}.$$

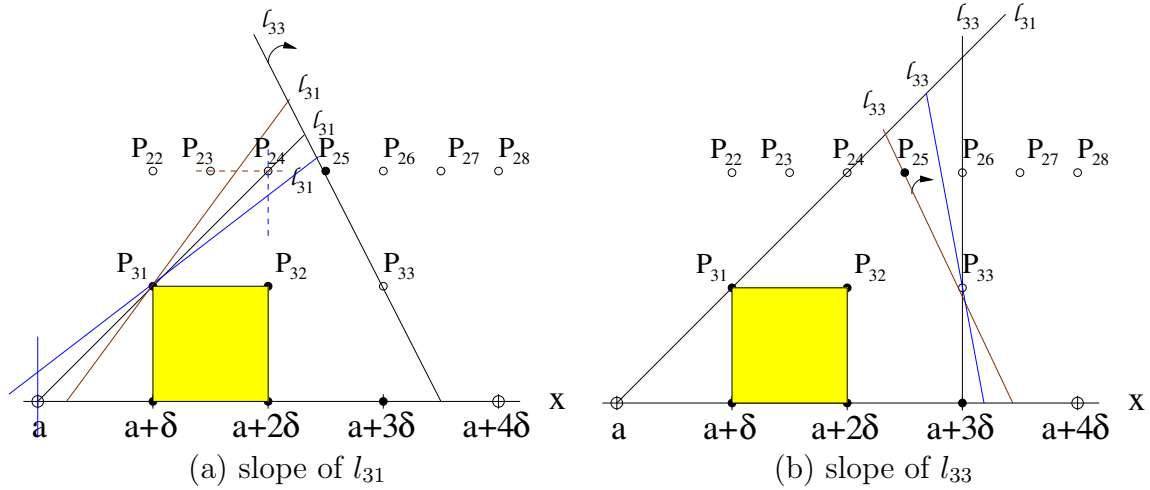


Figure 14: Subcase of Case 1-2, where  $P_{31}$  is on the boundary of  $\Omega'$  and  $P_{25} \in \Omega'$ . (a) demonstrates that  $P_{24}$  should not be below or above  $l_{31}$  in order to have a larger and feasible  $\Omega'$ ; (b) demonstrates that the larger the absolute value of the slope of  $l_{33}$  is, the larger the possible  $\Omega'$  is.

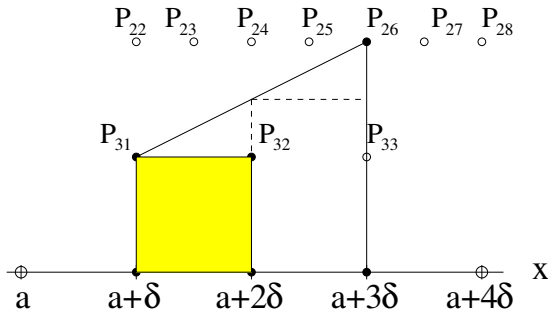


Figure 15: Subcase of Case 1-2, where  $P_{31}$  is on the boundary of  $\Omega'$  and  $P_{26} \in \Omega'$ . This case is impossible because we can find a higher dyadic rectangle in  $\Omega'$  with support  $(a+2\delta, a+3\delta)$ .

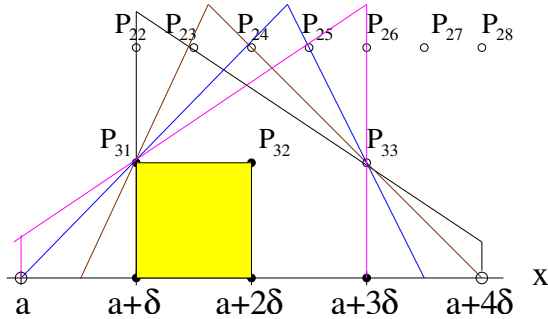


Figure 16: Subcase of Case 1-2, where  $P_{31}$  is on the boundary of  $\Omega'$  and none of  $P_{2j} \in \Omega'$

All the above are under the condition that  $P_{31}$  is on the boundary of  $\Omega'$ . On the other hand, when  $P_{32}$  is on the boundary of  $\Omega'$ , it is much simpler. Reader can refer to Figure 17 for more details. More specifically, since  $P_{46} \in \Omega'$  and  $P_{32}$  is on the boundary, none of  $P_{2x}(x \geq 2)$  is in  $\Omega'$  and the maximal possible  $\Omega'$  is bounded by the x-axis,  $l_{32}$ , which also passes through  $P_{46}$ , and the vertical line passes through point  $(a, 0)$ . Hence, we have

$$\frac{|MER|}{|\Omega'|} \geq \frac{2}{9}.$$

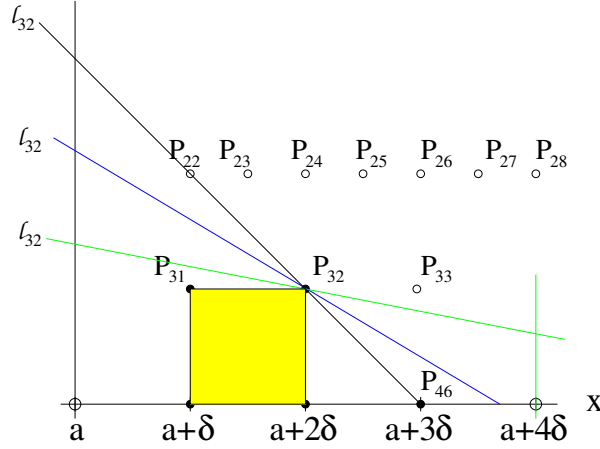


Figure 17: Subcase of Case 1-2, where  $P_{32}$  is on the boundary of  $\Omega'$ . In this case, the maximal  $\Omega'$  is bounded by the x-axis,  $l_{32}$  which also passes through  $P_{46}$ , and the vertical line passes through point  $(a, 0)$ .

We have finished the discussion about case C1-2. The analysis for the other cases is similar. We will just briefly go through the proof. Readers should be able to figure out the details by referring to the figures.

### 3.2.4 Case C1-5

For case C1-5, it can be subdivided as follows. Two points are critical: point  $P_{23}$  and point  $P_{24}$ . For these two points, at least one of them should be on the boundary of  $\Omega'$ .

We first assume that point  $P_{24}$  is on the boundary of  $\Omega'$  (Figure 18 and Figure 19). Hence,  $\Omega'$  is on the left of certain line  $l_{24}$ , which passes through  $P_{24}$ . Furthermore,  $P_{31} \notin \Omega'$ , otherwise, the MER has support  $(a + \delta, a + 2\delta)$ . So,  $\Omega'$  is on the right of the line  $l_{31}$ . Figure 18 shows that the possible  $\Omega'$  is larger when the slope of  $l_{31}$  is larger. Figure 19 details that  $l_{24}$  should pass through  $P_{33}$  (actually, a little below  $P_{33}$  since  $P_{33} \notin \Omega'$ ) in order to get larger  $\Omega'$ . Hence, the maximal possible  $\Omega'$  is surrounded by vertical line  $l_{31}$ , the x-axis, and  $l_{24}$

which also passes through  $P_{33}$ . So, we have

$$\frac{|MER|}{|\Omega'|} \geq \frac{2}{9}.$$

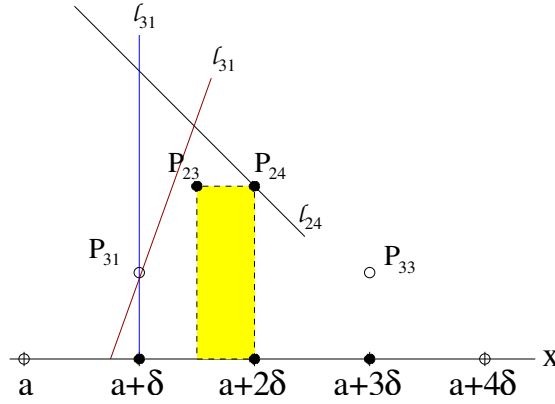


Figure 18: Subcase of Case 1-5, where  $P_{24}$  is on the boundary of  $\Omega'$ . For the slope of  $l_{31}$ ,  $\Omega'$  is on the right of  $l_{31}$ , and the possible  $\Omega'$  is larger when the slope of  $l_{31}$  is larger.

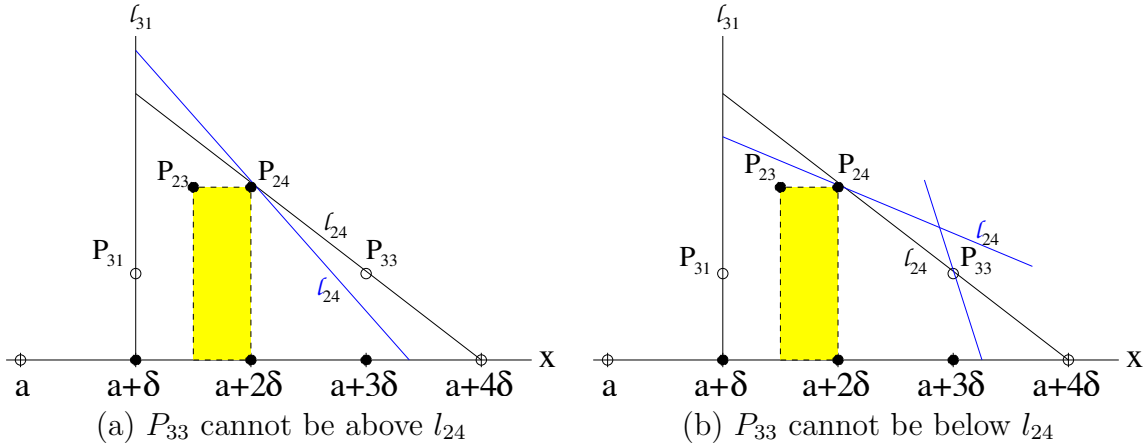


Figure 19: Subcase of Case 1-5, where  $P_{24}$  is on the boundary of  $\Omega'$ . For the slope of  $l_{24}$ , comparing with the case where  $P_{33}$  is on  $l_{24}$ , (a) demonstrates that the maximal possible  $\Omega'$  is smaller when  $P_{33}$  is above  $l_{24}$ ; (b) demonstrates that the maximal possible  $\Omega'$  is smaller when  $P_{33}$  is below  $l_{24}$ .

Next, if we assume point  $P_{23}$ , not point  $P_{24}$ , is on the boundary of  $\Omega'$  (Figure 20 and Figure 21). Hence,  $\Omega'$  is on the right of certain line  $l_{23}$ . Furthermore,  $P_{25}$  is not inside  $\Omega'$ , which means that there exists a line  $l_{25}$  such that  $\Omega'$  is on the left of it. Note  $l_{23}$  and  $l_{25}$  are critical here. From Figure 20, we observe that  $l_{25}$ , making a larger  $\Omega'$ , should pass through

$P_{33}$ . From Figure 21, we observe that  $l_{23}$ , making a larger  $\Omega'$ , should also pass through  $P_{31}$ . Hence, the maximal possible  $\Omega'$  is surrounded by these two specified lines and the x-axis. We have

$$\frac{|MER|}{|\Omega'|} \geq \frac{2}{9}.$$

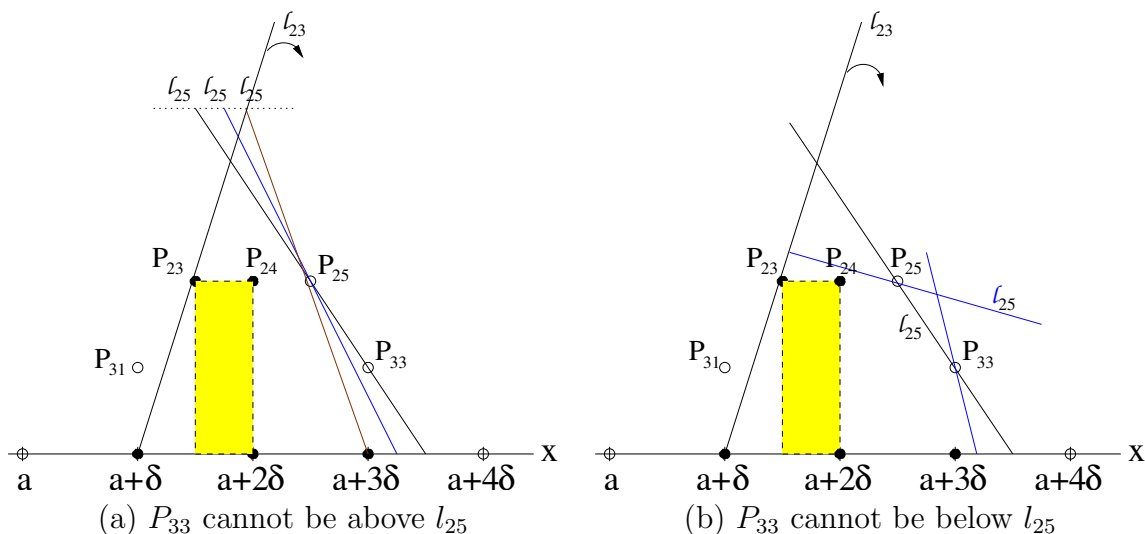


Figure 20: Subcase of Case 1-5, where  $P_{23}$  is on the boundary of  $\Omega'$ . We are considering the slope of  $l_{25}$ . Comparing with the case where  $P_{33}$  is on  $l_{25}$ , (a) demonstrates that the maximal possible  $\Omega'$  is smaller when  $P_{33}$  is above  $l_{25}$ ; (b) demonstrates that the maximal possible  $\Omega'$  is smaller when  $P_{33}$  is below  $l_{25}$ .

We finish case C1-5 and conclude that under this case, the theorem holds.

### 3.2.5 Case C2-2

Now we look at case C2-2, which is quite similar with case C1-2, but more complicated. The reason is we have more  $P_{2j}$ 's to be considered.

With an overview of this case (Figure 22), we know either  $P_{41}$  or  $P_{42}$  will be on the boundary of  $\Omega'$ . Due to the symmetry, these two are the same and we assume that  $P_{41}$  is on the boundary. Furthermore, among  $P_{24}$  up to  $P_{211}$ , at most one of them will be inside of  $\Omega'$ . Hence, we will have several subcases with respect to the state of each  $P_{2j}$ . We deal with them in the following.

If  $P_{24} \in \Omega'$  (Figure 23), we can prove this case is impossible since we can find a larger dyadic rectangle in  $\Omega'$  with support  $(a + \delta, a + 0.5\delta)$ . Similarly, the cases where  $P_{28} \in \Omega'$ , or  $P_{29} \in \Omega'$ , or  $P_{210} \in \Omega'$ , or  $P_{211} \in \Omega'$  contradict with the assumption of the MER. Hence, only 4 subcases need to be analyzed.

If  $P_{25} \in \Omega'$  (Figure 24 and Figure 25), then  $P_{26}$  is the closest point to  $P_{25}$  among the  $P_{2j}$ 's and  $P_{26} \notin \Omega'$ . Hence, in this case, the critical lines are  $l_{26}$  and  $l_{41}$ , where  $\Omega'$  is on the left side

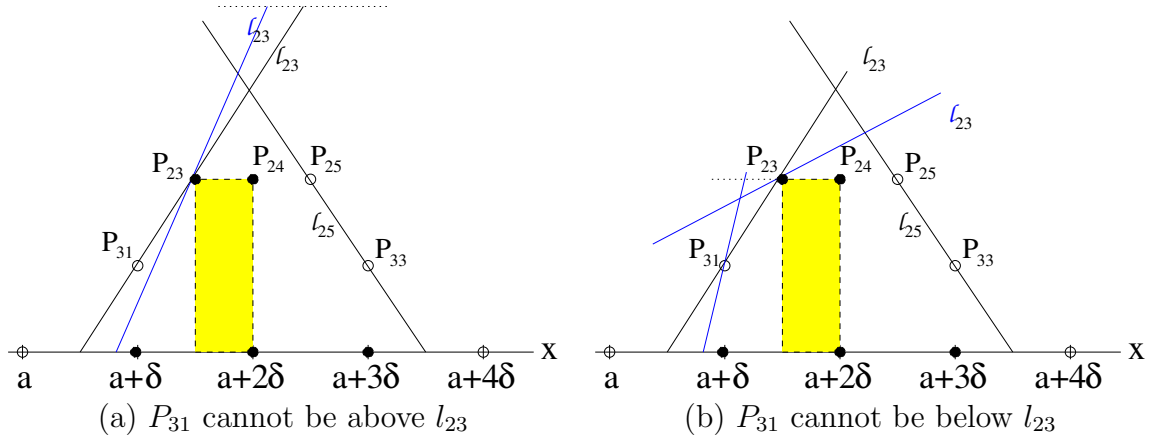


Figure 21: Subcase of Case 1-5, where  $P_{23}$  is on the boundary. We are considering the slope of  $l_{23}$ . Comparing with the case where  $P_{31}$  is on  $l_{23}$ , (a) demonstrates that the maximal possible  $\Omega'$  is smaller when  $P_{31}$  is above  $l_{23}$ ; (b) demonstrates that the maximal possible  $\Omega'$  is smaller when  $P_{31}$  is below  $l_{23}$ .

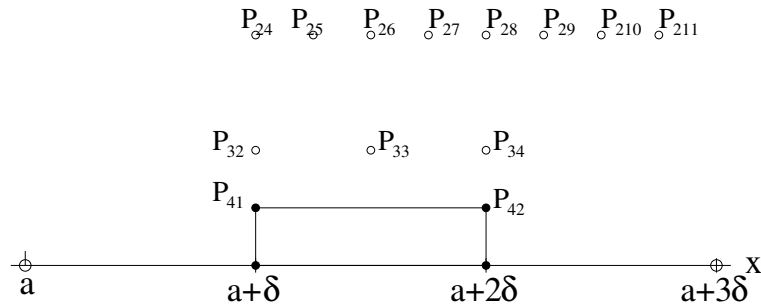


Figure 22: Case 2-2: an overview. Either  $P_{41}$  or  $P_{42}$  is on the boundary of  $\Omega'$ . We assume it is  $P_{41}$ . For points  $P_{2j}$ , at most one of them will be inside of  $\Omega'$ .

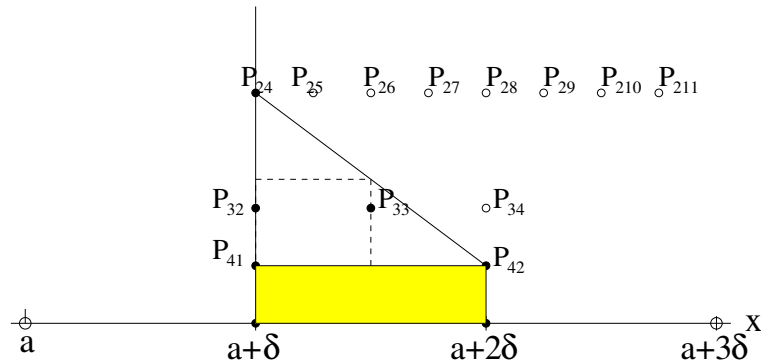


Figure 23: Subcase of Case 2-2, where  $P_{24} \in \Omega'$ . This case cannot happen since a larger embedded dyadic rectangle can be found.

of certain  $l_{26}$  and the right hand side of certain  $l_{41}$ . Figure 24 deals with the slope of  $l_{41}$  and Figure 25 deals with the slope of  $l_{26}$ . From Figure 24, we observe that the larger the slope of  $l_{41}$ , the larger the possible  $\Omega'$ . From Figure 25, we observe that  $l_{26}$  should pass through  $P_{34}$  to enclose a larger  $\Omega'$ . Hence, the maximal possible  $\Omega'$  is enclosed by the vertical  $l_{41}$ , the x-axis, and  $l_{26}$  that also passes through  $P_{34}$ . Hence, we have

$$\frac{|MER|}{|\Omega'|} \geq \frac{2}{9}.$$

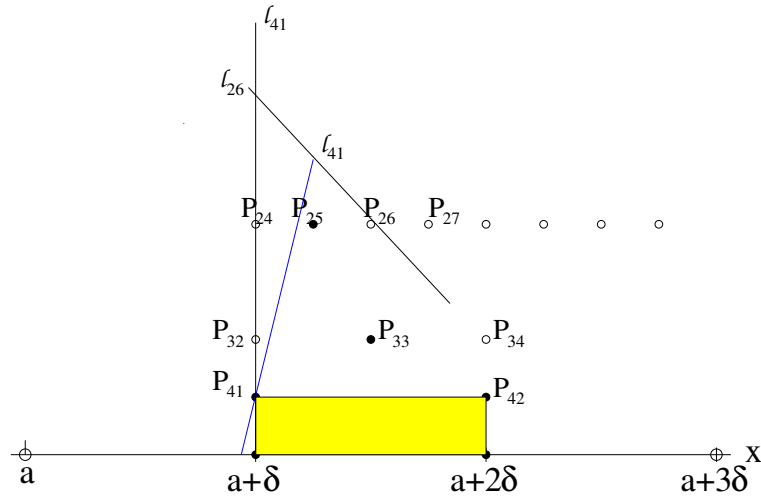


Figure 24: Subcase of Case 2-2, where  $P_{25} \in \Omega'$ . The slope of  $l_{41}$  is considered. It is clear that the larger the slope is, the larger the possible  $\Omega'$  is.

If  $P_{26} \in \Omega'$  (Figure 26), then  $P_{25}$  and  $P_{27}$  are not inside  $\Omega'$ . Recall  $P_{41}$  is on the boundary. Three lines are critical,  $l_{25}$ ,  $l_{27}$ , and  $l_{41}$ . Set  $\Omega'$  is on the right of  $l_{25}$  and  $l_{27}$  and on the left of  $l_{41}$ . Clearly from the figures, in order to enclose a larger possible  $\Omega'$ ,  $l_{27}$  should pass through  $P_{34}$  (Figure 26 (a)), and  $l_{25}$  and  $l_{27}$  are the same line (Figure 26 (b)). Therefore, the maximal possible  $\Omega'$  is surrounded by  $l_{27}$  that passes through  $P_{34}$ , line  $l_{41}$  that passes through  $P_{25}$ , and the x-axis. The relationship between the MER and the convex set  $\Omega'$  is

$$\frac{|MER|}{|\Omega'|} \geq \frac{4}{17} > \frac{2}{9}.$$

If  $P_{27} \in \Omega'$  (Figure 27),  $\Omega'$  are surround by lines  $l_{26}$ ,  $l_{34}$  and  $l_{41}$ . Obviously,  $l_{34}$  is vertical to the x-axis. From the figure, when the slope of  $l_{41}$  is larger, larger  $\Omega'$  could be enclosed. The slope of  $l_{26}$  can be found not changing the maximal possible  $\Omega'$ . Hence,

$$\frac{|MER|}{|\Omega'|_{\max}} = \frac{12}{49} > \frac{2}{9}.$$

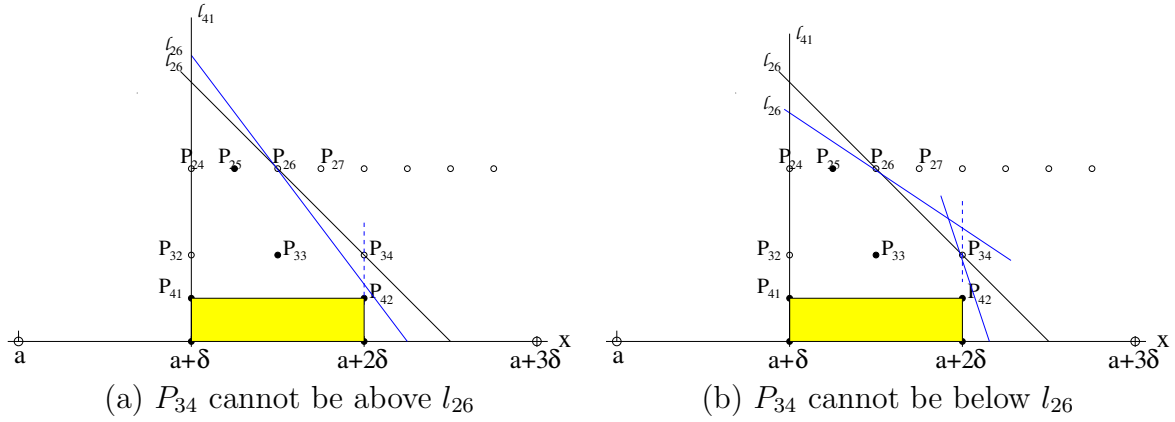


Figure 25: Subcase of Case 2-2, where  $P_{25} \in \Omega'$ . The slope of  $l_{26}$  is considered. Comparing with the case where  $P_{34}$  is on  $l_{26}$ , (a) demonstrates that the maximal possible  $\Omega'$  is smaller when  $P_{34}$  is above  $l_{26}$ ; (b) demonstrates that the maximal possible  $\Omega'$  is smaller when  $P_{34}$  is below  $l_{26}$ .

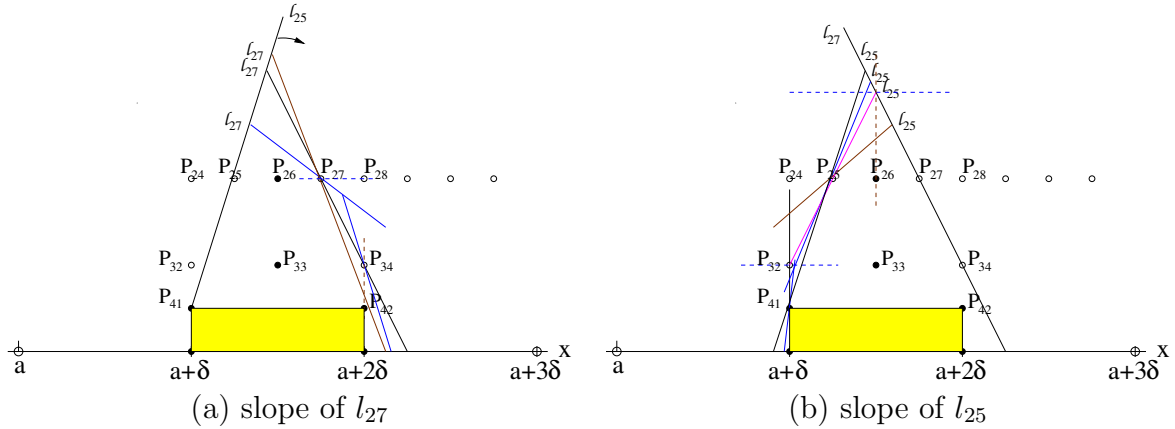


Figure 26: Subcase of case 2-2, where  $P_{26} \in \Omega'$ .  $\Omega'$  is surrounded by  $l_{25}$ ,  $l_{27}$  and  $l_{41}$ . (a) demonstrates that  $P_{34}$  cannot be below or above  $l_{27}$  in order to enclose a larger feasible  $\Omega'$ . (b) demonstrates that  $P_{41}$  cannot be below or above  $l_{25}$  in order to have a larger feasible  $\Omega'$ .

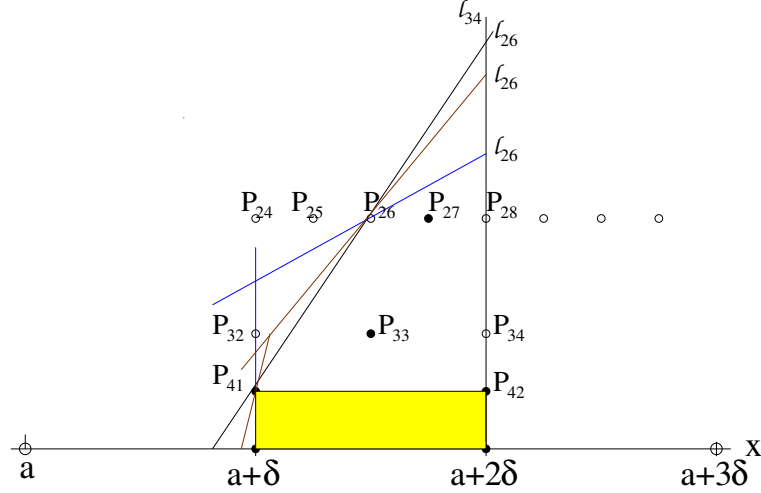


Figure 27: Subcase of Case 2-2, where  $P_{27} \in \Omega'$ . The maximal  $\Omega'$  is limited by vertical  $l_{41}$ , vertical  $l_{34}$ , the x-axis, and  $l_{26}$ . Slope of  $l_{26}$  won't change the area of the maximal  $\Omega'$  as long as it passes through  $P_{41}$ , or  $l_{41}$  is vertical.

If none of  $P_{2j} \in \Omega'$ , we can get more detailed subcases according to the status of  $P_{32}$ ,  $P_{33}$  and  $P_{34}$ . In each case, however, it is easy to verify the area of the MER is at least  $\frac{1}{4}$  of the area of  $\Omega'$ . This number is greater than  $\frac{2}{9}$ . We leave this for the readers.

Hence, case C2-2 is proved.

### 3.2.6 Case C2-3

In case C2-3, the MER has vertices  $P_{31}$  and  $P_{32}$  and support  $(a + 0.5\delta, a + \delta)$ . Therefore, either  $P_{31}$  or  $P_{32}$  is on the boundary of  $\Omega'$ .

If the point on the boundary is  $P_{32}$ , as shown in Figure 28, none of  $P_{2x}, x \geq 1$  in  $\Omega'$  since  $(a + 2\delta, 0)$  is inside  $\Omega'$ . Hence, the limiting boundary for the maximal  $\Omega'$  is: the vertical line passing  $(a, 0)$  ( $l_a$ ),  $l_{32}$  that passes  $P_{42}$ , and the x-axis. Please refer to Figure 28 for more details. Obviously, we have

$$\frac{|MER|}{|\Omega'|} \geq \frac{2}{9}.$$

On the other hand, if  $P_{31}$  is on the boundary of  $\Omega'$  (Figure 29), notice  $P_{33} \notin \Omega'$  and  $(a + 2\delta, 0) \in \Omega'$ . So,  $\Omega'$  is between  $l_{31}, l_{33}$  and the x-axis. We can easily check that when the largest possible  $\Omega'$  is enclosed,  $l_{33}$  passes through  $(a + 2\delta, 0)$  since  $P_{42} \notin \Omega'$ , and  $l_{31}$  is vertical. Hence, in this case,

$$\frac{|MER|}{|\Omega'|} \geq \frac{2}{9}.$$

Therefore, case C2-3 is checked.

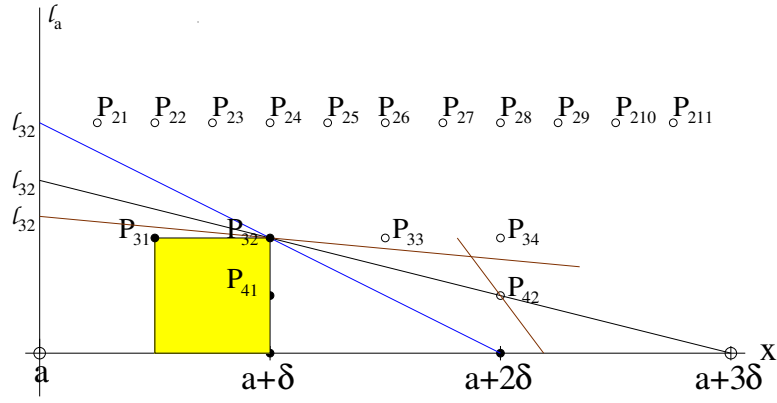


Figure 28: Subcase of Case C2-3, where  $P_{32}$  is on the boundary of  $\Omega'$ . None of  $P_{2j}$  is inside of  $\Omega'$ .  $\Omega'$  is surrounded by the vertical line  $l_a$ , the x-axis, and  $l_{32}$  that also passes  $P_{42}$ .

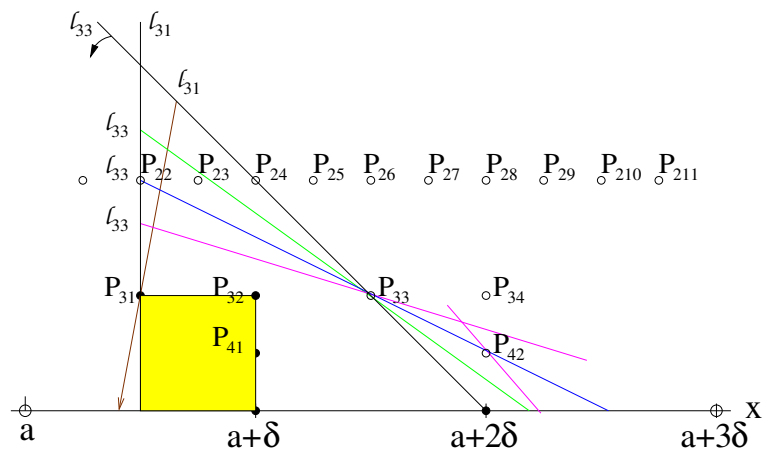


Figure 29: Subcase of Case C2-3, where  $P_{31}$  is on the boundary of  $\Omega'$ . Region  $\Omega'$  is between  $l_{31}$  and  $l_{33}$ . Note firstly, the larger the slope of  $l_{31}$ , the larger the possible  $\Omega'$ . Secondly,  $(a + 2\delta, 0)$  is below  $l_{33}$ . However, the larger the distance between them, the smaller the possible  $\Omega'$ .

### 3.2.7 Case C2-4

For C2-4, either  $P_{32}$  or  $P_{33}$  is on the boundary of  $\Omega'$ . The case while  $P_{33}$  is on the boundary is much easier than the other. We first consider the easier case. When  $P_{33}$  is on the boundary (Figure 30),  $P_{31} \notin \Omega'$ . Hence,  $\Omega'$  is between  $l_{31}$  and  $l_{33}$ . For line  $l_{31}$ , obviously, the larger the slope of  $l_{31}$ , the larger the possible  $\Omega'$ . Similar with the last subcase of C2-3, for  $l_{33}$ , , when  $l_{33}$  passes  $(a + 2\delta, 0)$ , the enclosed  $\Omega'$  has larger area. Hence, we have

$$\frac{|MER|}{|\Omega'|} \geq \frac{2}{9}.$$

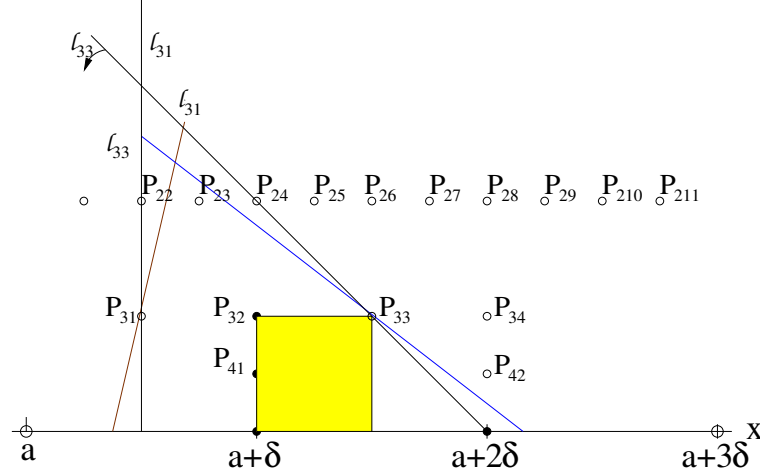


Figure 30: Subcase of Case C2-4, where  $P_{33}$  is on the boundary of  $\Omega'$ . Region  $\Omega'$  is between  $l_{31}$  and  $l_{33}$ . Note firstly, the larger the slope of  $l_{31}$ , the larger the possible  $\Omega'$  is. Secondly,  $(a + 2\delta, 0)$  is below  $l_{33}$ . However, the larger the distance between them, the smaller the possible  $\Omega'$ .

Meanwhile, if  $P_{32}$  is on the boundary of  $\Omega'$ , we can find an  $l_{32}$  such that  $\Omega'$  is on the right side of it. Furthermore, among  $P_{24}$  up to  $P_{27}$ , at most one of them will be in the  $\Omega'$ . So we will have several subcases with respect to the status of each  $P_{2j}$ ,  $4 \leq j \leq 7$ .

If  $P_{24} \in \Omega'$  (Figure 31), then  $P_{25} \notin \Omega'$ . Furthermore, we have  $P_{42} \notin \Omega'$ . Hence,  $l_{32}$ ,  $l_{25}$ , and  $l_{42}$  are crucial. Best states of these lines are:  $l_{32}$  is vertical to the x-axis,  $l_{25}$  is parallel to the x-axis, and  $l_{42}$  is vertical to the x-axis. Please refer to the figure. So,

$$\frac{|MER|}{|\Omega'|_{max}} > \frac{1}{4} > \frac{2}{9}.$$

If  $P_{25} \in \Omega'$  (Figure 32),  $\Omega'$  is bounded by  $l_{32}$ ,  $l_{26}$  and the x-axis. The best status is:  $l_{32}$  is vertical to the x-axis and  $l_{26}$  passes  $P_{42}$ , referring to the figure. Hence, we have

$$\frac{|MER|}{|\Omega'|} \geq \frac{12}{49} > \frac{2}{9}.$$

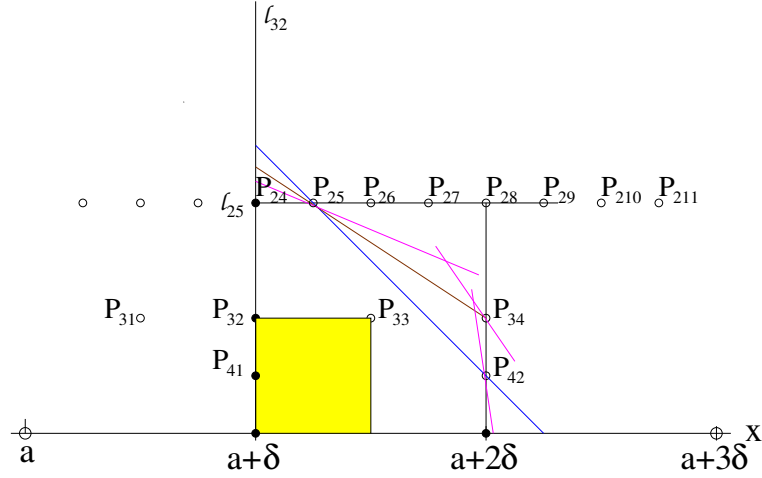


Figure 31: Subcase of Case C2-4, where  $P_{32}$  is on the boundary and  $P_{24} \in \Omega'$ .  $\Omega'$  is bounded by  $l_{32}$ ,  $l_{25}$ ,  $l_{42}$ , and the x-axis. Line  $l_{32}$  is vertical because both  $P_{24}$  and  $P_{32}$  are on the line.  $l_{25}$  being zero and  $l_{42}$  being vertical will enclose larger  $\Omega'$  that is applicable.

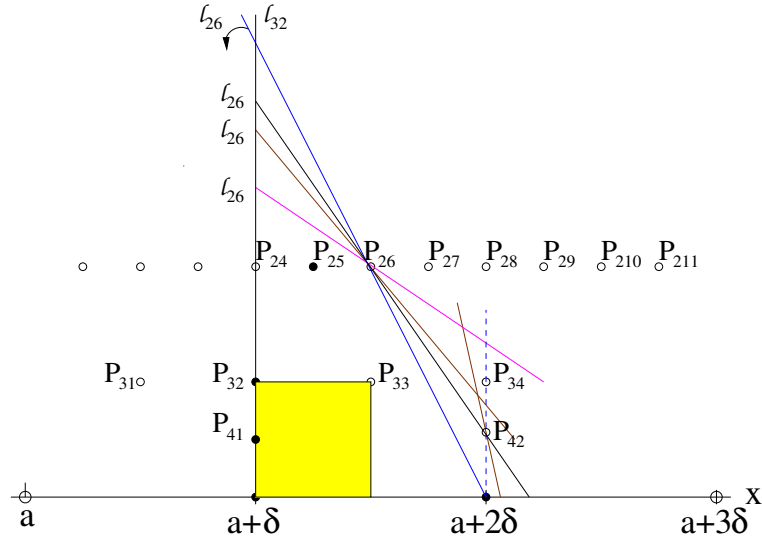


Figure 32: Subcase of Case C2-4, where  $P_{32}$  is on the boundary of  $\Omega'$  and  $P_{25} \in \Omega'$ .  $\Omega'$  is bounded by  $l_{32}$ ,  $l_{26}$ , and the x-axis. For  $l_{32}$ , the larger the slope is, the larger the possible enclosed  $\Omega'$  is. For  $l_{26}$ , point  $(a + 2\delta, 0)$  is below  $l_{26}$ . The larger the distance between them is, the larger the possible  $\Omega'$  is. Meanwhile,  $l_{26}$  is below  $P_{42}$  since  $P_{42}$  not in  $\Omega'$ . Hence, the best  $l_{26}$  passes  $P_{42}$ .

If  $P_{26} \in \Omega'$  (Figure 33),  $\Omega'$  is bounded by  $l_{32}$  and  $l_{27}$ . The best case, which includes a maximal possible  $\Omega'$ , is:  $l_{32}$  passing  $P_{25}$  and  $l_{27}$  passing  $P_{42}$ . Details can be found in the figure. Hence, we have

$$\frac{|MER|}{|\Omega'|} \geq \frac{15}{64} > \frac{2}{9}.$$

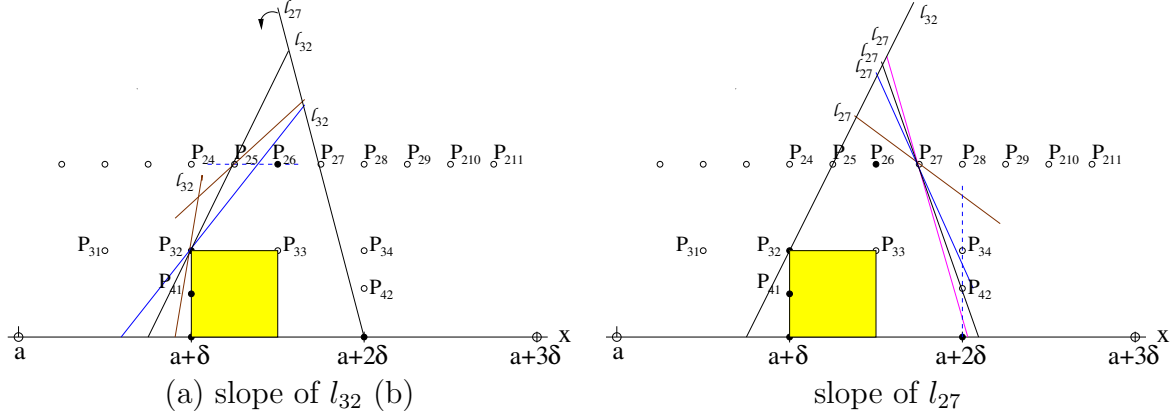


Figure 33: Subcase of Case C2-2, where  $P_{32}$  is on the boundary and  $P_{26} \in \Omega'$ .  $\Omega'$  is bounded by  $l_{32}$  and  $l_{27}$ . (a) indicates that in order to include a larger possible  $\Omega'$ ,  $l_{32}$  should pass  $P_{25}$ , or more correctly, slightly below  $P_{25}$ ; (b) indicates that  $l_{27}$  should pass  $P_{42}$  to include larger area.

If  $P_{27} \in \Omega'$  (Figure 34),  $\Omega'$  is bounded by  $l_{32}$  and  $l_{28}$ . The best case is:  $l_{32}$  passing  $P_{26}$  and  $l_{28}$  vertical. Details can be found in the figure. Again, we have

$$\frac{|MER|}{|\Omega'|} \geq \frac{2}{9}.$$

If none of  $P_{2x} \in \Omega'$ ,  $x = 4, 5, 6, 7$  (Figure 35),  $\Omega'$  could be surrounded by  $l_{32}$ ,  $l_{24}$ , and  $l_{28}$ . One of the best status is:  $l_{32}$  is vertical to the x-axis,  $l_{25}$  is parallel to the x-axis, and  $l_{42}$  is vertical to the x-axis. Hence,

$$\frac{|MER|}{|\Omega'|} > \frac{1}{4} > \frac{2}{9}.$$

### 3.2.8 Cases C2-5, C2-6, C2-7, C2-8, and C2-9

Cases C2-5 to C2-8 are similar to cases C1-3 and C1-4 (Figure 36 and Figure 37), where another embedded dyadic rectangle with larger area or with the same area but longer support can be found. Hence, these cases are either impossible or covered by other cases.

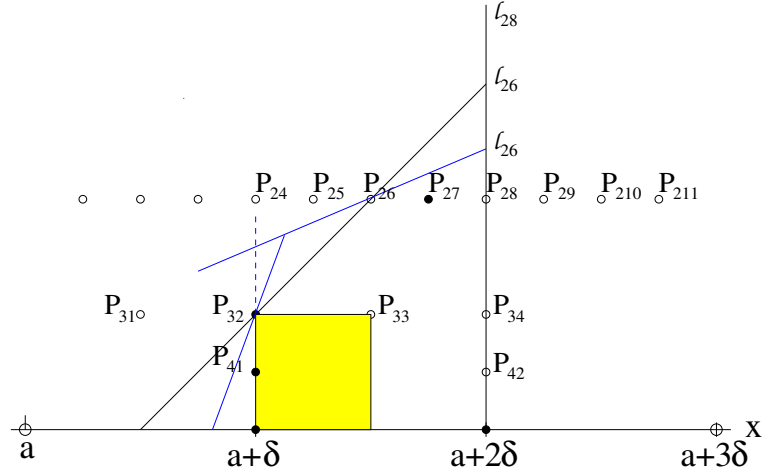


Figure 34: Subcase of Case 2-4, where  $P_{32}$  is on the boundary and  $P_{27} \in \Omega'$ . Region  $\Omega'$  is bounded by  $l_{32}$  and  $l_{28}$ . For  $l_{32}$ , when  $P_{26}$  is on it, the embedded area is larger than the area when  $P_{26}$  is not on the line. Line  $l_{28}$  should be vertical because  $P_{34}$  and  $P_{42}$  are not in  $\Omega'$ .

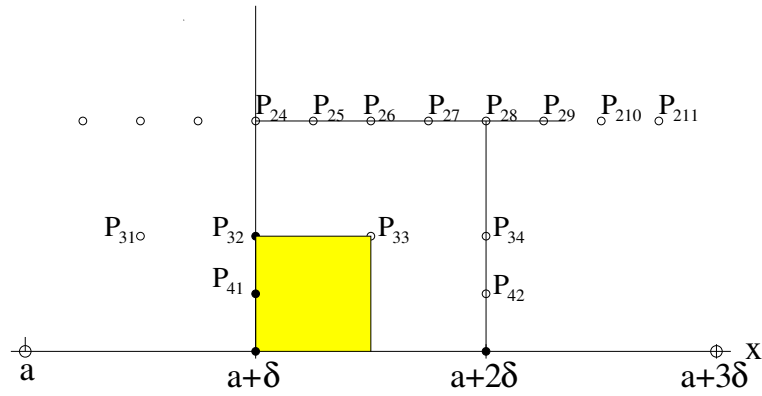


Figure 35: Subcase of Case C2-4, where  $P_{32}$  is on the boundary of  $\Omega'$  and none of  $P_{2j} \in \Omega'$ .  $\Omega'$  is surrounded by  $l_{32}$ ,  $l_{24}$ , and  $l_{28}$ . Line  $l_{28}$  is vertical because  $P_{34}$  is outside  $\Omega'$  and  $(a+2\delta, 0)$  is inside.  $l_{24}$  is horizontal because  $l_{28}$  is vertical and more area are supposed to be enclosed. Hence, given  $l_{28}$  and  $l_{24}$ , the slope of  $l_{32}$  can be any positive value as long as  $(a, 0)$  is above it.

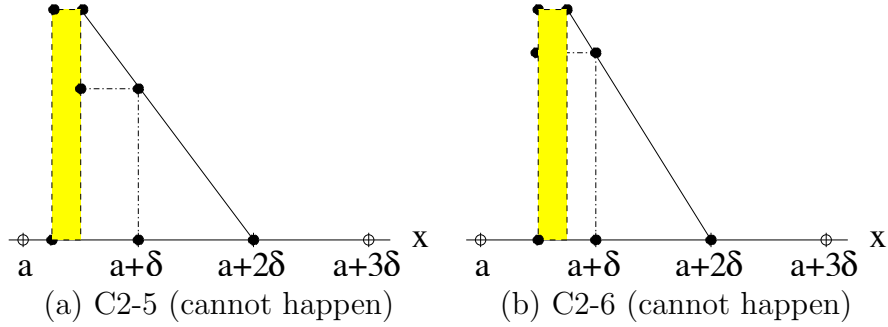


Figure 36: Case C2-5 & Case C2-6. Two impossible cases because a larger embedded dyadic rectangle can be found with support  $(a + 0.5\delta, a + \delta)$ .

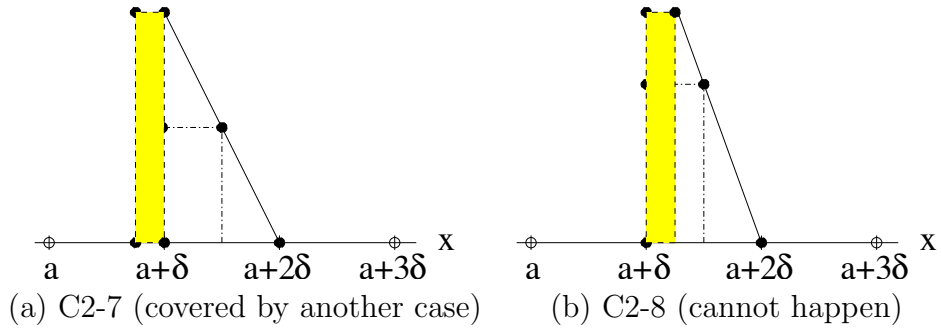


Figure 37: Case C2-7 & Case C2-8. (a) indicates that case C2-7 is covered by another case since comparing with the shaded part, a lower embedded rectangle with the same area but smaller height can be found; (b) indicates that case C2-8 is impossible because a larger dyadic rectangle can be found.

### 3.2.9 Case C2-9

This case is almost the same as case C1-5. For point  $P_{25}$  and point  $P_{26}$ , at least one of them should be on the boundary of  $\Omega'$ . We first assume that point  $P_{26}$  is on the boundary (Figure 38 and Figure 39). Hence, there exists a line  $l_{26}$  such that  $\Omega'$  is on the left side of this line. Furthermore, we have  $P_{32} \notin \Omega'$ , so there is a line  $l_{32}$  such that  $\Omega'$  is on the right side of it. The best choice for such  $l_{32}$  and  $l_{26}$  is that  $l_{32}$  is vertical (Figure 38) and  $l_{26}$  passing  $P_{34}$ . Therefore, we have

$$\frac{|MER|}{|\Omega'|} \geq \frac{2}{9}.$$

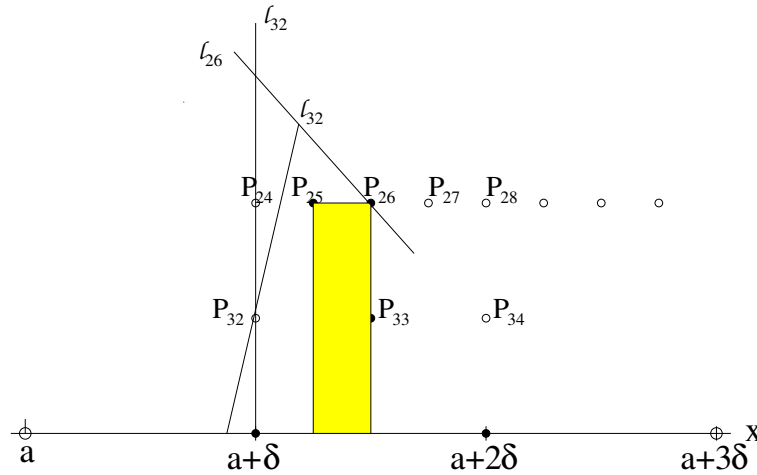


Figure 38: Subcase of Case C2-9, where  $P_{26}$  is on the boundary of  $\Omega'$ . Region  $\Omega'$  is between  $l_{32}$  and  $l_{26}$ . The slope of  $l_{32}$  is considered here. The line should be vertical such that the enclosed area is larger.

On the other hand, when  $P_{25}$  is on the boundary of  $\Omega'$  (Figure 40 and Figure 41). Lines  $l_{27}$  and  $l_{25}$  are crucial, because  $\Omega'$  is between them. From those two figures, the enclosed possible  $\Omega'$  is maximized if  $l_{27}$  passes  $P_{34}$  (Figure 40) and  $l_{25}$  passes  $P_{32}$  (Figure 41). Hence, we have

$$\frac{|MER|}{|\Omega'|} \geq \frac{2}{9}.$$

Based on all the above, we have proved the Theorem 3.

## 4 Discussion

Similar works, regarding constants related to multiscale methods in other scenarios, can be found in [2, 3].

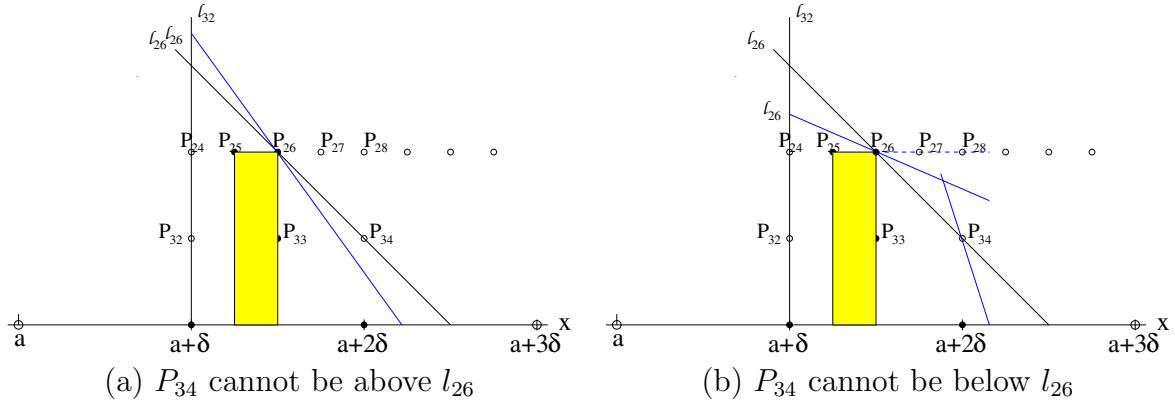


Figure 39: Subcase of Case 2-9, where  $P_{26}$  is on the boundary of  $\Omega'$ . Region  $\Omega'$  is between  $l_{32}$  and  $l_{26}$ . The slope of  $l_{26}$  is considered here. In order to include more area, (a) indicates that  $P_{34}$  cannot be above  $l_{26}$  and (b) indicates that  $P_{34}$  cannot be below  $l_{26}$ .

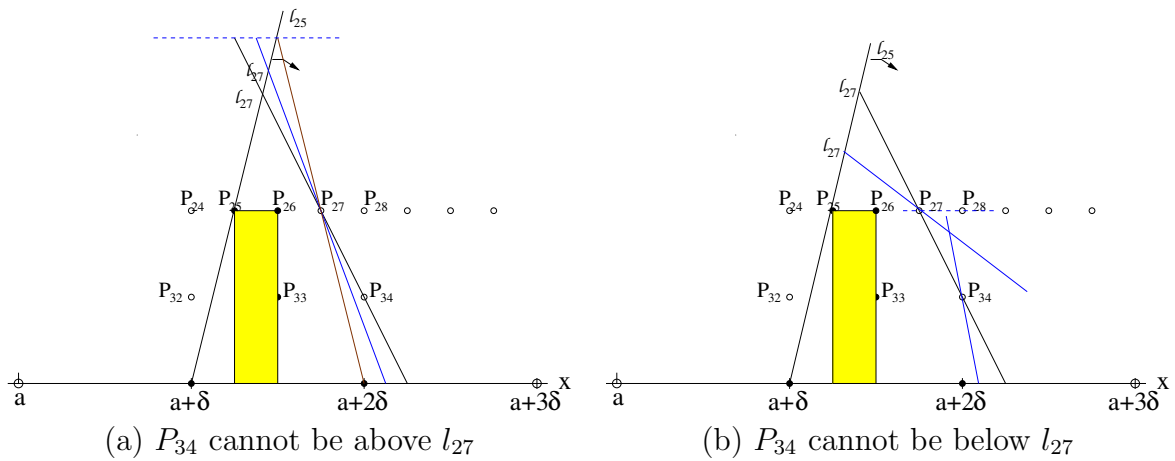


Figure 40: Subcase of Case 2-9, where  $P_{25}$  is on the boundary. Consider the slope of  $l_{27}$ , (a) indicates that the enclosed area is smaller if  $P_{34}$  is above  $l_{27}$ ; (b) indicates that the enclosed area is smaller if  $P_{34}$  is below  $l_{27}$ .

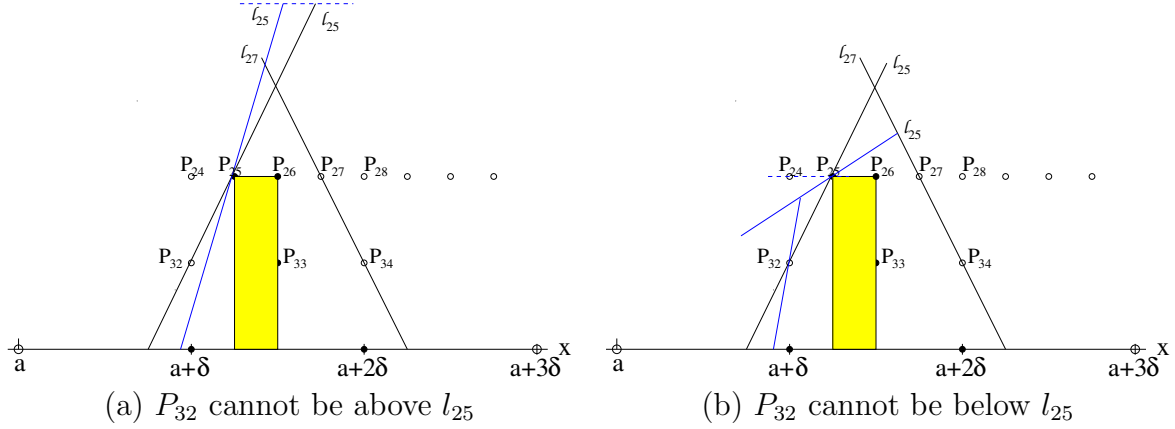


Figure 41: Subcase of Case 2-9, where  $P_{25}$  is on the boundary. We consider the slope of  $l_{25}$ . (a) indicates that the enclosed area is smaller if  $P_{32}$  is above  $l_{25}$ ; (b) indicates that the enclosed area is smaller if  $P_{32}$  is below  $l_{25}$ .

The main theorem of this paper is used in [5] to justify a multiscale detection algorithm, which has applications in problems such as rooftop detection [4, 7], lesion detection [9, 8], and contamination detection [11] in CryoEM [10].

There might be simpler classification of the possible configurations, which could lead to a simpler proof. Since our objective is finding the constant “2/9”, we choose not to invest our energy on pursuing a simpler proof; even though it can be an interesting geometric problem by itself.

## References

- [1] E. Arias, D. L. Donoho, and X. Huo. Near-optimal detection of geometric objects by fast multiscale methods. *IEEE Trans. Information Theory*, 51(7):2402–2425, July 2005.
- [2] X. Huo. Exact lower bound for proportion of maximally embedded beamlet. *Applied Mathematics Letters*, 18(5):529–534, May 2005.
- [3] X. Huo. Minimax correlation between a line segment and a beamlet. *Statistics & Probability Letters*, 72(1):71–81, April 2005.
- [4] M. A. Maloof, P. Langley, T. O. Binford, R. Nevatia, and S. Sage. Improved rooftop detection in aerial images with machine learning. *Machine Learning*, 53(1-2):157–191, October–November 2003.
- [5] X. S. Ni and X. Huo. On the detectability of convex-shaped inhomogeneous objects in digital images. Submitted, Oct. 2005. Available from the authors.

- [6] Xuelei (Sherry) Ni. *New results in detection, estimation, and model selection*. PhD thesis, Georgia Institute of Technology, Atlanta, GA, December 2005. Available at <http://etd.gatech.edu/>.
- [7] S. Noronha and R. Nevatia. Detection and description of buildings from multiple aerial images. In *Proceedings of the 1997 Conference on Computer Vision and Pattern Recognition (CVPR '97)*, pages 588–594, 1997.
- [8] J. Qi. Analysis of lesion detectability in Bayesian emission reconstruction with non-stationary object variability. *IEEE Transactions on Medical Imaging*, 23(3):321–329, 2004.
- [9] J. Qi and R. H. Huesman. Theoretical study of lesion detectability of MAP reconstruction using computer observers. *IEEE Trans. Med. Imaging*, 20(8):815–822, August 2001.
- [10] M. van Heel, B. Gowen, R. Matadeen, E. V. Orlova, R. Finn, T. Pape, D. Cohen, H. Stark, R. Schmidt, M. Schatz, and A. Patwardhan. Single-particle electron cryo-microscopy: towards atomic resolution. *Quarterly Reviews of Biophysics*, 33(4):307–369, November 2000.
- [11] Y. Zhu, B. Carragher, and C. S. Potter. Contaminant detection: improving template matching based particle selection for cryo-electron microscopy. In *Proceedings of the IEEE International Symposium on Biomedical Imaging*, pages 1071–1074, Arlington VA, April 2004.